

Scatter of measured K_{IC} related to the scatters of local parameters X_f , σ_f and ε_{pc}

Jian Hong Chen* and Rui Cao

Department of Material Science and Engineering and State Key laboratory of Non-ferrous Metals of Lanzhou
University of Technology, Lanzhou, China

* Corresponding author: zchen@lut.cn

Abstract 42 values of K_{IC} measured at -100°C are related to the measured values of local fracture stress σ_f and the fracture distance X_f by the formula: $K_{IC} = \beta^{-(N+1)/2} X_f^{1/2} [\sigma_f^{(1+N)/2N} / \sigma_y^{(1-N)/2N}]$. The scatters of K_{IC} caused by σ_f or X_f are assessed separately at constant values of X_f or σ_f . It is found that at a constant X_f the scatter of K_{IC} induced by the scatter of σ_f accounts for only 20% of the total scatter, while at a nearly constant σ_f the scatter of K_{IC} caused by the scatter of X_f can reach almost 100% of the total scatter of K_{IC} . It means that the effect of the scatter of X_f on the scatter of K_{IC} is much larger than that of σ_f . This idea is opposite to the assumption widely accepted in local approach that the distribution of various sizes of the carbide particles which present various values of σ_f is the main event in the statistical calculation. Instead, the random distribution of (X_f) of weakest particles with the lowest values of σ_f should be considered as the determining factor in statistical assessment for the cleavage fracture.

Keywords Scatter of K_{IC} , Local fracture stress σ_f , Fracture distance X_f , Fracture strain ε_{pc}

1. Introduction

The relationships between global toughness, such as the critical stress intensity factor K_{IC} and the critical values of parameters specified in the micromechanism of cleavage fracture, such as local fracture stress σ_f , fracture distance X_f and fracture strain ε_{pc} , are of great significance. These relationships offer the bases for establishing the statistical model (such as the local approach) which uses the micro-parameters to predict the global failure probability.

For pre-cracked specimens of a normalized C-Mn steel the relations between the global toughness measured in cleavage-fractured specimens and the critical values of local parameters ε_{pc} , σ_f and X_f had been discussed in a previous paper[1], where the discussion started from the Eq. (1) [2]

$$K_{IC} = \beta^{-(N+1)/2} X_k^{1/2} \left[\sigma_f^{(1+N)/2N} / \sigma_y^{(1-N)/2N} \right], \quad (1)$$

β is the amplitude of HRR crack tip stress singularity [3,4]

Here this equation is modified to Eq. (2) by substituting X_f for X_k .

$$K_{IC} = \beta^{-(N+1)/2} X_f^{1/2} \left[\sigma_f^{(1+N)/2N} / \sigma_y^{(1-N)/2N} \right], \quad (2)$$

In Eq. (1) X_k is the ‘characteristic distance’ [5], In Eq. (2) X_f is the fracture distance i.e. the measured distance from the cleavage initiation site to the blunted precrack tip. In Eq. (2) the factor

$$F = X_f^{1/2} \left[\sigma_f^{(1+N)/2N} / \sigma_y^{(1-N)/2N} \right], \quad (3)$$

correlates the global fracture toughness K_{IC} to the local parameters σ_f and X_f .

In following, the relations will be analyzed using the data of Table 1 which were measured in 42 specimens at -100°C . The C-Mn steel specimens were normalized, austenized at 900°C for 2 hours then air cooled. The uniform microstructure is composed of the ferrite grains of $9.3\mu\text{m}$ in average size and $22\mu\text{m}$ for the largest grains and the pearlite colonies around $3.2\mu\text{m}$ in the average size and $20\mu\text{m}$ for the largest.

Table 1 fracture toughness-associated parameters measured in COD tests of a normalized C-Mn steel

Test No.	P _{Gy} (N)	P _f (N)	T=100°C σ _y =470MPa σ _{max} =1880MPa Q _{max} =4.0 DMS/δ _c =1.25 N=0.21										Mark
			δ _c (μm)	X _f (μm)	X _f ^{1/2} (mm ^{1/2})	X _f /δ _c	σ _f (MPa)	ε _{pc}	σ _m /σ _e	F (MPa m ^{-1/2})	K _{IC}	d (μm)	
Y02	8036	9016	114	102	0.32	0.89	1852	0.0458	2.41	241.9	131.0	4.0	L
Y40	8330	8673	74	158	0.4	2.14	1795	0.0058	2.81	276.3	105.5	3.0	R
Y41	7840	8820	121	131	0.36	1.08	1861	0.0369	2.62	276.0	134.9	3.0	L
Y05	7644	8036	72	60	0.24	0.83	1852	0.0678	2.10	181.4	104.1	11.3	L
Y26	7448	8232	100	120	0.35	1.2	1861	0.0311	2.73	268.3	122.7	4.5	L
Y31	7644	7840	53	75	0.27	1.41	1847	0.0140	3.10	202.5	89.3	3.8	R
Y36	8036	8330	64	139	0.37	2.17	1791	0.0052	2.85	254.0	98.1	4.4	R
Y25	7644	8526	111	90	0.3	0.81	1852	0.0673	2.12	226.8	129.2	3.2	L
Y35	7350	8330	128	175	0.42	1.37	1852	0.0180	3.05	317.5	138.8	7.5	R
Y11	8428	9212	117	119	0.34	1.02	1800	0.0241	2.57	232.6	132.7	7.5	L
Y47	8036	8232	55	86	0.29	1.56	1842	0.0184	3.06	215.8	91.0	5.4	R
Y13	—	7350	20	63	0.25	3.15	1617	0.0050	2.65	127.9	54.9	8.6	R
Y21	—	7840	22	62	0.25	2.82	1678	0.0052	2.72	142.2	57.5	3.8	R
Y44	7448	7644	52	112	0.33	2.15	1790	0.0075	2.96	226.2	88.4	7.5	R
Y43	7840	7840	26	78	0.28	3	1645	0.0063	2.64	153.6	62.5	6.6	R
Y15	—	6468	10	69	0.26	6.9	1391	0.0036	2.27	58.1	38.8	5.4	R
Y22	6860	7448	131	169	0.41	1.29	1861	0.0219	2.90	314.3	140.4	6.1	L
Y42	7840	8134	81	75	0.27	0.93	1861	0.0458	2.84	188.4	110.4	4.8	L
Y19	7546	7840	80	131	0.36	1.64	1842	0.0133	3.03	267.9	109.7	8.3	R
Y12	8036	8232	73	113	0.34	1.55	1833	0.0184	3.08	249.5	104.8	6.5	R
Y27	7350	7350	42	16	0.13	0.38	1810	0.1829	1.62	92.0	82.3	3.0	L
Y23	6953	7252	56	66	0.26	1.18	1861	0.0233	2.71	199.3	91.8	3.8	L
Y14	7546	7546	33	69	0.26	2.09	1860	0.098	2.94	199.0	70.5	6.3	R
Y16	7840	8036	72	169	0.41	2.35	1758	0.0040	2.81	266.8	104.1	3.0	R
Y30	7644	8330	82	96	0.31	1.17	1861	0.0240	2.70	237.6	111.1	8.1	L
Y04	—	8036	29	138	0.37	4.75	1490	0.0035	2.44	149.5	66.1	3.5	R
Y37	8428	8624	77	124	0.35	1.61	1833	0.0183	3.08	256.8	107.6	6.5	R
Y38	8722	8918	47	10	0.32	2.13	1795	0.0080	2.90	221.1	84.1	2.7	R
Y33	8330	8526	36	93	0.3	2.58	1840	0.0057	2.66	222.6	73.6	3.8	R
Y10	8036	8036	30	67	0.26	1.68	1763	0.0052	2.93	170.5	67.2	3.2	R
Y17	—	7546	14	60	0.24	4.29	1513	0.0042	2.51	101.3	45.9	2.9	R
Y03	—	7350	12	30	0.17	2.5	1767	0.0046	2.83	112.2	42.5	3.8	R
Y1	—	5330	10	20	0.14	2	1734	0.0059	2.80	87.5	38.8	*	R
Y2	—	6270	12	17	0.13	1.42	1838	0.0186	2.80	96.1	42.5	*	R
Y3	—	7500	17	85	0.29	5	1466	0.0035	2.45	111.8	50.6	*	R
Y4	—	7690	22	50	0.22	2.27	1706	0.0051	2.92	134.4	57.5	*	R
Y5	8560	8670	35	43	0.21	1.23	1875	0.0254	2.69	164.5	72.6	*	L
Y6	8570	8670	36	44	0.21	1.22	1875	0.0245	2.72	164.5	73.6	*	L
N01	6370	7640	132	25	0.16	0.19	1800	0.4257	2.57	111.4	140.9	6.0	L
N23	8430	8430	34	20	0.14	0.59	1828	0.1166	1.71	101.9	71.5	3.7	L
N06	5684	6080	54	51	0.23	0.94	1852	0.0443	2.84	173.9	90.2	4.3	L
N21	8530	8530	30	0	0	0	1743	0.9727	0.60	0.0	67.2	2.3	L

No: specimen number ; T: test temperature; P_y: yield load; P_f: fracture load; σ_y: yield stress; δ_c: critical value of COD; X_f: distance from cleavage initiation site to blunted precrack tip ; σ_f: local fracture stress; ε_{pc}: critical plastic strain; σ_m/σ_e: critical stress triaxiality; F=X_f^{1/2}{σ_f^{(1+N)/2N}/σ_y^{(1-N)/2N}}, K_{IC}: critical stress intention factor, d: diameter of particle triggering cleavage; Mark: denoting the distance of cleavage initiation site relative to that of peak stress; L: distance shorter than that of peak stress position DMS, X_f < DMS; R: distance longer than that of peak stress position DMS, X_f > DMS;

2. Relationship between K_{IC} and factor $F=X_f^{1/2}[\sigma_f^{(1+N)/2N}/\sigma_y^{(1-N)/2N}]$

Fig.1 depicts the relationship between the measured values of K_{IC} and the factor (3) $F=X_f^{1/2}[\sigma_f^{(1+N)/2N}/\sigma_y^{(1-N)/2N}]$. As seen in Fig.1 in a general trend K_{IC} increases with F in a linear pattern, however the variation of K_{IC} values measured at -100°C is quite large. The highest value of K_{IC} of $140.9\text{MPam}^{-1/2}$ is as large as 363% of the lowest value of $38.8\text{MPam}^{-1/2}$. The absolute difference (scatter) reaches $102\text{MPam}^{-1/2}$. The scatter of measured values of K_{IC} at an identical value of F accounts for $55.8\text{MPam}^{-1/2}$ which implies that besides the X_f and σ_f a factor has significant effect on the values of K_{IC} .

Three parallel lines divide the K_{IC} -distributing zone to two areas: in the upper area all points \bullet represent the crack initiation site (X_f) locating on the left side of the peak stress position DMS, $X_f < \text{DMS}$ (shown in Fig.4). In the lower area, all points \circ represent the crack initiation site (X_f) locating on the right side of DMS, $X_f > \text{DMS}$ (Fig.4). As discussed in authors' previous work [1] the higher ε_{pc} makes the crack initiation site to the left side of DMS, where the plastic strain is higher, As seen in Fig.1, at same F values, all specimens marked by \bullet present values of K_{IC} higher than that of specimens marked by \circ . That is, the measured values of K_{IC} are higher for points (marked by \bullet) which represent the crack initiation site (X_f) located at the left side of DMS due to the higher ε_{pc} . This observation demonstrated the effects of higher ε_{pc} on the increments of the scatter of K_{IC} . In addition in the upper area, the scatter of measured values of K_{IC} (the vertical distance between the upper and the median lines) accounts for about $34.1\text{MPam}^{-1/2}$ which is considered to be caused by variation of ε_{pc} at fixed F . The scatter of measured values of K_{IC} in the lower area accounts for about $21.7\text{MPam}^{-1/2}$ which is considered to be caused by some intrinsic factors, such as the errors made in measurements and also by variations of ε_{pc} which varies in a range with values lower than that to cause the crack initiation site locating on the left side. The scatter in the lower area is appreciably lower than the scatter in the upper area.

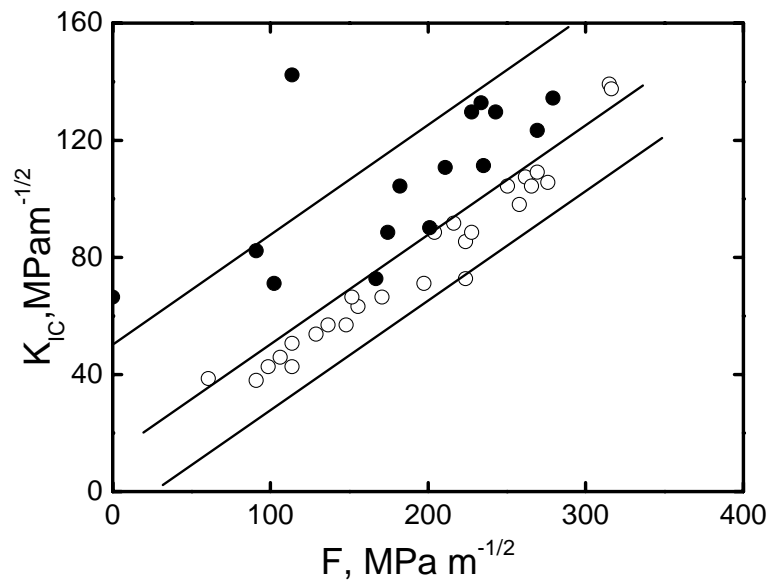


Figure 1. K_{IC} plotted against $F=X_f^{1/2}[\sigma_f^{(1+N)/2N}/\sigma_y^{(1-N)/2N}]$ for a normalized C-Mn steel,
 \bullet for X_f on the left side of DMS, \circ for X_f on the right side of DMS

In following sub-sections, relationships between global toughness and critical values of microscopic parameters of the normalized C-Mn steel are analyzed in the order of σ_f , X_f and ε_{pc} .

3 Effects of σ_f

For investigating the effect of σ_f on the scatter of measured values of K_{IC} , Fig.2 is drawn, which shows the plots of K_{IC} against the square root of the fracture distance, $X_f^{1/2}$, using the data of Table 1. Then Fig.2 is compared with Fig.1 where the K_{IC} is plotted against $F = X_f^{1/2} [\sigma_f^{(1+N)/2N} / \sigma_y^{(1-N)/2N}]$. Because in Fig.1, the product of $X_f^{1/2}$ and σ_f (in the term of $[\sigma_f^{(1+N)/2N} / \sigma_y^{(1-N)/2N}]$) is fixed at an abscissa value, the effects of the variations of $X_f^{1/2}$ and σ_f on the K_{IC} values offset to each other, the effect of the variation of σ_f alone is minor. While in Fig.2 at a fixed $X_f^{1/2}$, only the σ_f is varied, thus the difference of scatters presented between Fig.1 and Fig.2 at a fixed abscissa is attributed to the scatters of the σ_f . The scatter of K_{IC} at a fixed $X_f^{1/2}$ reaches 77.5MPam^{-1/2} in Fig.2. Comparing this value with the scatter of 55.8MPam^{-1/2} at a fixed F in Fig.1, the total scatter of σ_f from 1391MPa to 1875MPa (demonstrated in the Table 1) causes about 21.7MPam^{-1/2} in the scatter of K_{IC} , which accounts for about 28% of the scatter of 77.5MPa m^{-1/2} at a fixed $X_f^{1/2}$ and only 21% in whole scatter of 102MPam^{-1/2} measured at -100°C for the 42 specimens of the normalized C-Mn steel.

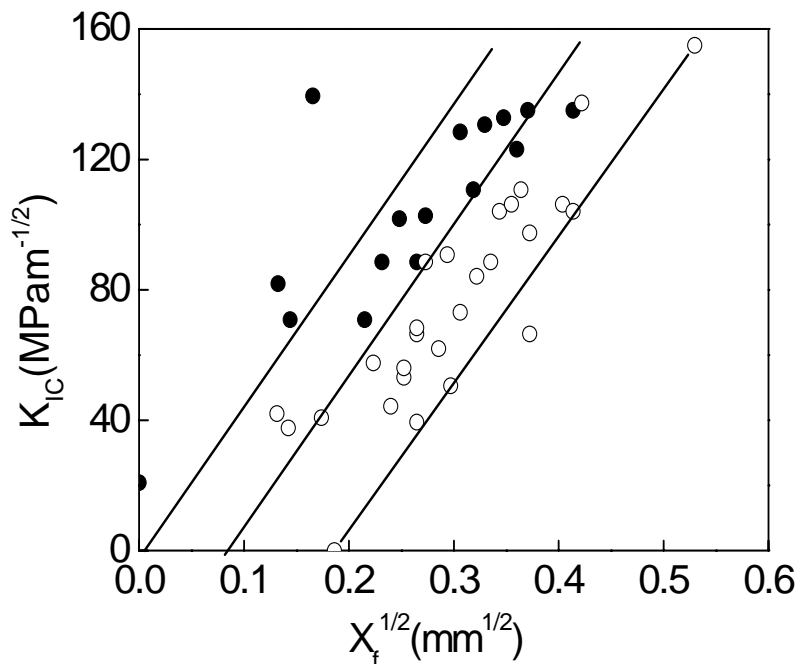


Figure 2. K_{IC} plotted against $X_f^{1/2}$ for a normalized C-Mn steel
● for X_f on left side of DMS ○ for X_f on right side of DMS, (Chen, 1998)

For further analyses, in Fig.2 one median line is also drawn, which divides the K_{IC} -distributing zone to two areas: in the upper area all points ● represent the crack initiation site (X_f) locating at the left side of DMS and have higher K_{IC} . The scatter in this area (the vertical distance between the upper and median lines) of measured values of K_{IC} reaches about 34.1MPam^{-1/2} at a fixed X_f which is almost the same in Fig.1. It means that the scatter of σ_f has little influence on the scatter of K_{IC} in the upper area. In the lower area, all points ○ represent the crack initiation site (X_f) locating at right side of DMS and have lower K_{IC} . The scatter in this lower area (the vertical distance between the lower and median lines) of measured values of K_{IC} accounts for about 43.4MPam^{-1/2} which is 21.7 MPam^{-1/2} larger than that in Fig.1 and the difference is considered to be caused by variation of the σ_f in term of $[\sigma_f^{(1+N)/2N} / \sigma_y^{(1-N)/2N}]$ at a fixed X_f .

In summary, the effects of the variation of σ_f from 1391MPa to 1875MPa at a fixed X_f induce 21.7 MPam^{-1/2} i.e. only 20% increase in scatter of K_{IC} and manifests itself in the lower area where the normal stress predominates the cleavage fracture process. Therefore it is not reasonable for a statistical model to be based on the statistical distribution of the local fracture stress σ_f i.e. on the

microcrack size distribution.

4 Effects of X_f

In Fig.2 K_{IC} measured at -100°C is plotted against $X_f^{1/2}$ for the normalized C-Mn steel. It is seen that with increasing X_f , the K_{IC} values increase remarkably. The K_{IC} increases from $38.7\text{MPa m}^{-1/2}$ to $140.7\text{MPa m}^{-1/2}$ (along one parallel line) at the variation of X_f from $16\mu\text{m}$ to $175\mu\text{m}$. For further analyses of the effect of X_f , Fig.3 is drawn with the plots of measured values of K_{IC} against the factor

$$F' = \left[\sigma_f^{(1+N)/2N} / \sigma_y^{(1-N)/2N} \right] \quad (4)$$

so that at a fixed abscissa the σ_f is fixed while the X_f is able to vary and to show its effect on the K_{IC} .

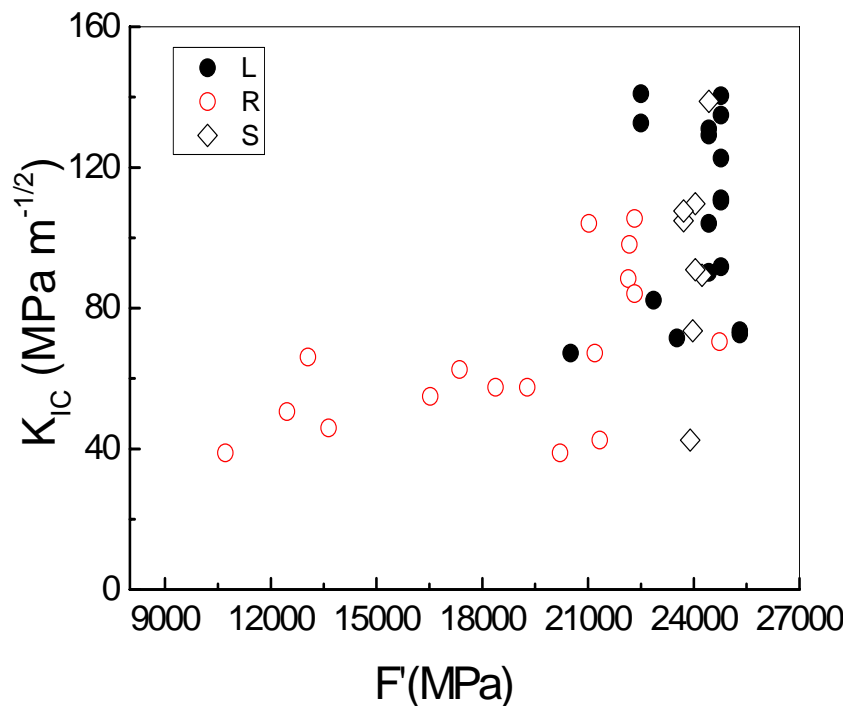


Figure 3. K_{IC} plotted against $F' = [\sigma_f^{(1+N)/2N} / \sigma_y^{(1-N)/2N}]$ for a normalized C-Mn steel
 ● for X_f on left side of DMS ○ for X_f on right side of DMS

Fig.3 shows a unique shape distinct from Fig.1 and Fig.2. Unlike Fig. 1 and Fig.2, the distribution of scatter cannot be delimited between two parallel lines. In the region of F' less than 20000 MPa the scatter of K_{IC} is low and can be neglected. In the region of F' higher than 20000 MPa the scatter of measured values of K_{IC} is large and shows a uniform pattern. The points ● representing the crack initiation site (X_f) locating on the left side of DMS mix uniformly with points ○ and ◇ representing the crack initiation site (X_f) locating on the right side of DMS. It means that at a fixed abscissa of F' the effects of ε_{pc} on the scatter of K_{IC} are incorporated into the effects of X_f . It is worth noticing that at a near constant abscissa (marked by ◇) the scatter covers almost the whole scale in measurement. Table 2 lists the values of K_{IC} for specimens with F' distributed in a narrow region (from 23709MPa to 24424MPa). The corresponding points are marked by ◇ in Fig.3. All points represent the crack initiation site (X_f) locating on the right side of DMS.

Table 2. Data of K_{IC} , X_f and correlated parameters

T=100°C $\sigma_y=470\text{MPa}$ $\sigma_{max}=1880\text{MPa}$, $Q_{max}=4.0$ N=0.21							
No	F (MPa m ^{-1/2})	F' (MPa)	σ_f (MPa)	X_f (μm)	$X_f^{1/2}$ (mm ^{1/2})	K_{IC} (MPam ^{-1/2})	Mark
Y35	317.5	24424.7	1852	175	0.42	138.8	R
Y19	267.9	24046.7	1842	131	0.36	109.7	R
Y37	256.8	23709.7	1833	124	0.35	107.6	R
Y12	249.5	23709.7	1833	113	0.34	104.8	R
Y47	215.8	24046.7	1842	86	0.29	91.0	R
Y31	202.5	24235.2	1847	75	0.27	89.2	R
Y33	222.6	23971.5	1840	93	0.30	73.6	R
Y2	96.1	23896.5	1838	17	0.13	42.5	R

NO: specimen number ; T: test temperature; N: work hardening exponent, σ_y : yield stress;
 $F=X_f^{1/2}[\sigma_f^{(1+N)/2N}/\sigma_y^{(1-N)/2N}]$, $F'=[\sigma_f^{(1+N)/2N}/\sigma_y^{(1-N)/2N}]$, σ_f : local fracture stress; X_f : distance from cleavage initiation site to blunted precrack tip ; K_{IC} : critical stress intention factor, Mark: denoting the distance of peak stress position site relative to that of peak stress; L: distance shorter than that of peak stress position; R: distance longer than that of peak stress position;

As revealed by Fig.3 and Table 2, in a very narrow range of variation of F' (from 23896kgmm⁻² to 24424 kgmm⁻²) the increase of K_{IC} from 42.5 MPam^{-1/2} to 138.8 MPam^{-1/2} reaches 96.3MPam^{-1/2} which almost covers total scatter of measured values of K_{IC} . Because in this narrow range of F' the σ_f almost keeps constant (varies from 1833MPa to 1852MPa) and the effect of ϵ_{pc} on the scatter of K_{IC} is incorporated into the effect of X_f , the increase of K_{IC} can only be attributed to the increases with X_f . The small variation of X_f from 17 μm to 175 μm causes the increase of K_{IC} from 42.5 MPam^{-1/2} to 138.8MPam^{-1/2} almost covering total scatter of measured values of K_{IC} . Thus, the effect of X_f on the scatter of K_{IC} is of major significant. This phenomenon also indicates that the macro-index of the fracture toughness, K_{IC} , can not represent a true material's property, instead it is a parameter dependent on the location of the precrack. The same argument has been held by Pineau and Tanguy[6].The K_{IC} has not a unique value but has a minimum value which is determined by the minimum fracture distance X_f .

5. Effects of ϵ_{pc}

As discussed in section 2 the major effects of high ϵ_{pc} manifest their selves in making the cleavage crack initiation site closer to the pre-crack tip (move to left side of DMS) and then increasing K_{IC} . In previous work [1] for revealing the effect of ϵ_{pc} the X_f in the factor F for points locating on the left side is replaced by X_o the distance of a corresponding point on the right branch of the normal stress distribution curve with the same local fracture stress σ_f (as shown in Fig.4).

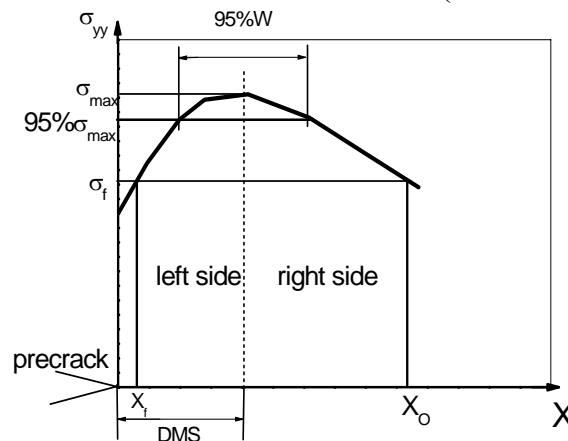


Figure 4. Schematics showing replacing X_o for X_f [1]

Fig.5 plots K_{IC} against F in which the $X_o^{1/2}$ (marked by \circ), is substituted for $X_f^{1/2}$ (marked by \bullet) i.e. $F=X_o^{1/2}[\sigma_f^{(1+N)/2N}/\sigma_y^{(1-N)/2N}]$ and the major effect of ϵ_{pc} is evaded. Comparing Fig.1 with Fig.5 it is apparent that when the major effect of ϵ_{pc} is evaded the relation between K_{IC} and F is more stringed. The scatter in K_{IC} at an identical F is reduced to about $21.7\text{MPam}^{-1/2}$ in Fig.5 from $55.8\text{MPam}^{-1/2}$ in Fig.1. It means that through moving the cleavage site from the right side to the left side the scatter in ϵ_{pc} (0.0035 to 0.1829) could have caused about $34.1\text{MPam}^{-1/2}$ in scatter of K_{IC} .

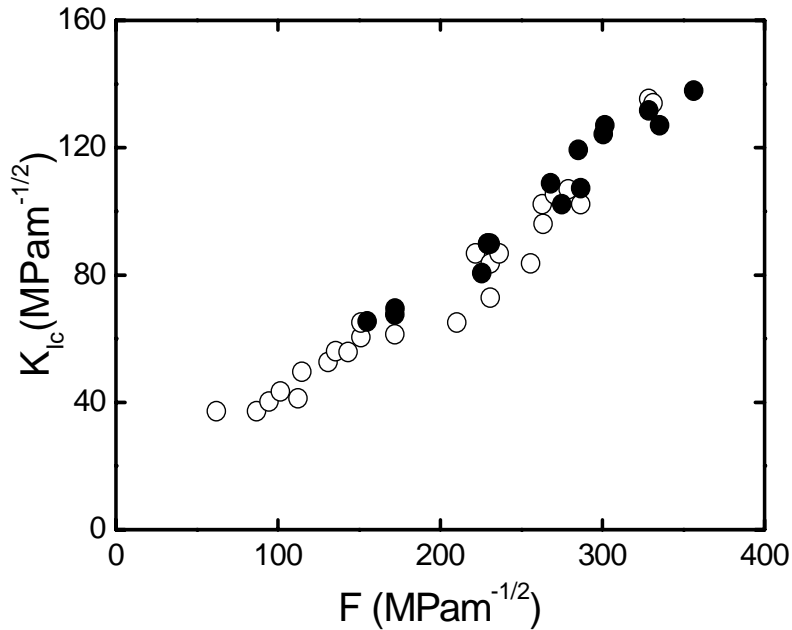


Figure 5. K_{IC} plotted against $F=X_o^{1/2}[\sigma_f^{(1+N)/2N}/\sigma_y^{(1-N)/2N}]$ for a normalized C-Mn steel \bullet for X_f originally on left side of DMS \circ for X_o originally on right side of DMS

Fig.6 plots K_{IC} against $X_o^{1/2}$, where X_o is modified from X_f and the major effect of variation of ϵ_{pc} is evaded. Comparing it with Fig.2, it also shown that the scatter at same $X_o^{1/2}$ could be much reduced from $77.5\text{MPam}^{-1/2}$ to about $43.4\text{MPam}^{-1/2}$, part of which (about $21.7\text{MPam}^{-1/2}$) is caused by the variation of σ_f . Thus both Fig.5 and Fig.6 show the effects of the variation of ϵ_{pc} (0.0035 to 0.1829) on the scatter of K_{IC} account for about $34.1\text{MPam}^{-1/2}$.

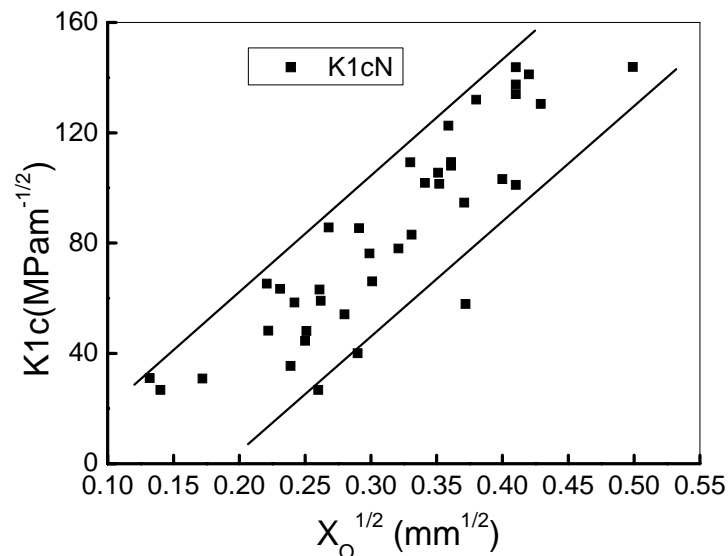


Figure 6. K_{IC} plotted against $X_o^{1/2}$ for a normalized C-Mn steel [1]

In summary, the relationship between fracture toughness K_{IC} and parameters of micromechanism of cleavage fracture X_f , σ_f and σ_y of a C-Mn normalized steel can be generally described by the formula

$$K_{IC} = \beta^{-(N+1)/2} X_f^{1/2} \left[\sigma_f^{(1+N)/2N} / \sigma_y^{(1-N)/2N} \right], \quad (2)$$

Here the work hardening exponent N is taken as 0.21, and the amplitude of HRR crack tip stress singularity β is about 6.14.

As shown in Fig.1, the measured values of K_{IC} exhibit a linear pattern of distribution against the term $F = X_f^{1/2} [\sigma_f^{(1+N)/2N} / \sigma_y^{(1-N)/2N}]$ with a slope content of 1/3. The total scatter of K_{IC} reaches $102 \text{ MPam}^{-1/2}$ and at a fixed F value it reaches $55.8 \text{ MPam}^{-1/2}$.

The scatters in K_{IC} caused by the micro-parameters in micromechanism of cleavage fracture are summarized as follows:

X_f , variation from $17 \mu\text{m}$ to $175 \mu\text{m}$ at fixed σ_f produce scatter of $96.3 \text{ MPam}^{-1/2}$ accounting for 95% in total scatter of $102 \text{ MPam}^{-1/2}$

σ_f , variation from 1391 MPa to 1875 MPa at fixed X_f produce scatter $21.7 \text{ MPam}^{-1/2}$ accounting for 21% in total scatter of $102 \text{ MPam}^{-1/2}$

ε_{pc} , variation from 0.0035 to 0.1829 at fixed σ_f produce scatter $34.1 \text{ MPam}^{-1/2}$ accounting for 34% in total scatter of $102 \text{ MPam}^{-1/2}$

Among these three main micro-parameters, the X_f is the major significant factor in production of scatter in measured values of K_{IC} . Thus, in a statistical model, the variation of X_f should be taken into account as the main factor firstly. The effect of ε_{pc} present in moving the X_f . In case the variation of X_f (including on both left and right sides) has been taken as the main factor, the effect of ε_{pc} is diminished. In common cases, the σ_f is a stable parameter and its scatter is within $\pm 10\%$, which causes about 20% of the scatter of K_{IC} so its effect is minor. Therefore, it is unreasonable to take the distribution of σ_f as the main event in a statistic model.

Acknowledgements

This work was financially supported by National Nature Science Foundation of China (No. 51035004 and 51265028).

References

- [1] J. H. Chen, G. Z. Wang, On scattering of measured values of fracture toughness parameters. *Inter. J. Fract*, 94(1998)33-49.
- [2] D. A. Curry, Cleavage micromechanisms of crack extension in steels. *Metal. Sci*, 14(1980)319-326.
- [3] J. W. Hutchinson, Plastic stress and strain field at a crack tip. *J. Mech. Phys. Solids*, 16(1968)13-31.
- [4] J. R. Rice, G. R. Rosengren, Plain strain deformation near a crack tip in a power-law hardening material. *J. Mech. Phys. Solids*, 16(1968)1-12.
- [5] R.O. Ritchie, J. F. Knott, J. R. Rice, On the relationship between critical tensile stress and fracture toughness in mild steel. *J. Mech. Phys. Solids*, 21(1973) 395-410.
- [6] A. Pineau and B. Tanguy, Advances in cleavage fracture modeling in steels: Micromechanical, numerical and multiscale aspects, *Comptes Rendus Physique*, 11, (2010) 316-325